Mater. Res. Soc. Symp. Proc. Vol. 1059 © 2008 Materials Research Society 1059-KK01-06

Interplay between Morphology and Surface Transport in Nanopatterns Produced by Ion-Beam Sputtering

Rodolfo Cuerno[1], Javier Muñoz-García[2], Mario Castro[3], Raúl Gago[4], and Luis Vázquez[5]
[1]Departamento de Matemáticas and GISC, Universidad Carlos III de Madrid, Avenida de la Universidad 30, Leganés (Madrid), E-28911, Spain
[2]Departamento de Matemáticas and GISC, Universidad de Castilla la Mancha, Ciudad Real, E-13071, Spain
[3]Escuela Técnica Superior de Ingeniería (ICAI) and GISC, Universidad Pontificia Comillas de Madrid, Madrid, E-28015, Spain
[4]Centro de Microanálisis de Materiales, Universidad Autónoma de Madrid, Madrid, E-28049, Spain
[5]Instituto de Ciencia de Materiales de Madrid, Consejo Superior de Investigaciones Científicas, Madrid, E-28049, Spain

ABSTRACT

A "hydrodynamic" model has been proposed to describe nanopattern formation and dynamics on amorphous surfaces eroded by ion-beam sputtering (IBS), that relates to descriptions of pattern formation in macroscopic systems such as aeolian sand dunes. At variance with previous continuum models of the morphology of ion-sputtered surfaces, the dynamics of the species that diffuse along the surface is coupled in a natural way to that of the surface height. We report recent results for this model, considering normal and oblique ion incidence, for both fixed and rotating targets, and include comparison to recent experiments on silicon. Effective interface equations can be obtained, that generalize the anisotropic Kuramoto-Sivashinshy equation through additional conserved Kardar-Parisi-Zhang type nonlinear terms. In general dot or ripple patterns form, that later evolve exhibiting complex nonlinear dynamics. Thus, we observe interrupted coarsening behavior such that, for normal incidence, domains of hexagonally ordered structures appear, that compare favorably with those obtained in many experiments of nanodot formation by IBS. In other parameter regions, this short-range ordered patterns coexist with long range disorder and kinetic roughening. For oblique incidence, a ripple pattern is generically obtained that also shows interrupted coarsening and other nonlinear features like non-uniform transverse motion, again reproducing experimental observations.

INTRODUCTION

Materials nanostructuring by ion-beam sputtering (IBS) has received increased attention in recent years [1-3], due to the potential of this bottom-up procedure for applications in Nanotechnology, and also due to the interesting issues it arises in the wider context of Pattern Formation at submicrometer scales [4]. In these experiments, a target is irradiated by a collimated beam of energetic ions (typical energies being in the keV range) that impinge onto the former under a well defined angle of incidence. Although routinely employed since long for many diverse applications within Materials Science (material implantation, sample preparation, etc.) the capabilities of this technique for efficient nanopatterning have been recognized only recently, see references in [1-3]. Thus, it induces self-organized regular ripple (at oblique ion

incidence) or dot (at normal ion incidence, or arbitrary incidence onto rotating targets) nanopatterns over large areas (up to 1 cm^2) on metal, semiconductor, and insulator surfaces after a few minutes of irradiation. Interestingly, the main features of this pattern formation process seem to be largely independent of the type of ions (even those inducing reactive sputtering) and targets employed, as long as the latter amorphize under irradiation (the case of metals falls outside this class, and will not be addressed here, but see [1-3]).

Many experimental studies have allowed to assess the formation of a pattern due to the variation of the sputtering efficiency (sputtering yield) with the local surface geometry, in competition with additional relaxation mechanisms, such as surface diffusion and other. Albeit with many deviations, the main features of this process can be largely summarized as follows: a periodic surface pattern initially forms during a transient associated with fast (exponential) growth of its amplitude (as quantified e.g. by the surface roughness), after which the roughness grows at a much lower rate and/or saturates to a stationary value. In general, in-plane order of the pattern increases with sputtering time. Moreover, often the pattern wavelength l coarsens with time to finally saturate. In the stationary state, the surface morphology may display a varying degree of long-wavelength disorder in the height of its various features (such as domains of nanostructures with short to medium range order), featuring in some cases the properties of kinetic roughening. Morphological features such as symmetry of the arrangement, detailed shape (conical, sinusoidal, etc.) of the nanostructures, rates of roughening and coarsening, etc. depend on experimental parameters, such as ion and target species, incidence angle θ, average energy and flux, temperature and other. In general, the behaviors for ripple patterns seem to be better established than for dot patterns. This may be related to the fact that dot pattern production by IBS is relatively recent. On the other hand, both types of IBS patterns share many qualitative features, which suggests description within a common framework.

Typically, the nanopatterns induced by IBS fully evolve in macroscopic time and length scales (minutes and several microns, respectively). It is at these scales where, e.g., interaction among ripples can be seen to lead to order improvement with sputtering time or, rather, to eventual disorder in heights. Although detailed knowledge on the phenomenon of sputtering is rapidly and consistently developing through (microscopic) Molecular Dynamic and Monte Carlo studies (see references e.g. in [2,3]), macroscopic scales are not currently within reach for these methods. Actually, the wide separation between the microscopic time scales typical of events that take place in the target during irradiation (like surface diffusion attempts, or relaxation of single collision cascades, in the order of ps), and the large-scale response of its surface morphology, recall a similar separation between microscopic and collective motion in the case of e.g. fluid dynamics. Thus, it is natural to expect [4] that some continuum description in the spirit of, say, the Navier-Stokes equations might be appropriate in the case of nanopattern formation by IBS. The advantage of continuum descriptions, if available, is that they provide compact descriptions of complex physical phenomena. Moreover, they are frequently more efficient computationally for the study of large scale properties, whose generic properties they can faithfully describe, see references in [4]. Nevertheless, for the type of non-equilibrium phenomena which are our present focus, the relevant continuum equations are most times non-linear, their study requiring either analytical approximations or numerical simulations.

Pioneering such an approach, Sigmund [5] showed that the topography of the surface can indeed influence the magnitude of the erosion rate. He proposed that the total velocity of erosion at a surface point is proportional to the integral of the space distribution of energy deposition, that for amorphous or amorphizable materials is accurately described by a Gaussian distribution.

As he already noted, this description implies the occurrence of a morphological instability since valleys are excavated more quickly that crests amplifying initial height differences. Moreover, he suggested that an alternative process that flattens the surface must exist such as atomic migration, in order to correct this instability. The theory of Sigmund is the basis for most of the later continuum approaches to IBS nanopatterning. In principle, as a *theory of sputtering*, it is known to have limitations. Within the present range of energies, two of the most conspicuous ones refer to the behavior of the sputtering yield for large incidence angles, and crystalline targets. Related with the former, Sigmund's theory predicts an steady increase of the yield with θ, and fails to describe the well-known decrease at glancing incidence due to projectile reflection and channeling effects. Nevertheless, recent continuum studies [6] have shown that improved distributions accounting for this effect do not modify qualitatively the morphological predictions to be derived below. Similarly, Sigmund's theory is limted as applied to crystalline solids. Thus, different distributions must be considered, as done e.g. in [7] for the particular case of Cu targets. However, as seen in this work, again these modifications do not alter the qualitative morphological implications of the continuum theories to be described below, which justifies (at least for temperatures at which Ehrlich-Schwoebel barriers do not dominate surface diffusion [1-3]) the strong similarities in nanopattern formation by IBS on metals, as compared with amorphizable targets. As a *morphological theory*, again Sigmund's has limitations: it does not predict the alteration of the morphology during the process for scales much larger than the average ion penetration depth, *a*, and, as surface diffusion is not considered, the pattern wavelength remains of the same order; the effects of surface shadowing or redeposition are not considered; it does not predict the time evolution of the morphology and how it affects the rate of erosion. Thus, additional physical mechanisms and a more detailed description of the surface height are needed in order to derive a morphological theory with an increased predictive power.

CONTINUUM APPROACHES: ONE FIELD

Sigmund's formula for the local velocity of erosion constitutes an ideal starting point in order to put forward a continuum description of these non-equilibrium systems. This is so because one may add different contributions to it corresponding to additional physical mechanisms, as indeed has been done. The insight of Bradley and Harper (BH) [8] was that, under reasonable physical approximations, Sigmund's formula becomes a closed time (t) evolution equation for a single physical field, the target height $h(x, y, t)$ above point (x, y) on a reference plane. It is within such (simple) single-field approach that most of the recent continuum descriptions have circumscribed themselves. However, this program will be seen later to encounter physical and mathematical limitations. Within the BH approach, the variation in the height of the surface is assumed smooth at scales that are comparable with the average penetration depth a. Taking the x direction to be the projection of the ion beam onto the uneroded target and expanding h as a function of the surface geometry up to linear order in the surface curvatures, they obtained a closed evolution equation that reads

$$\partial_t h = -v_0 + \gamma_x \partial_x h + \nu_x \partial_x^2 h + \nu_y \partial_y^2 h - B\nabla^4 h\,, \qquad (1)$$

where, given that $\nu_x, \nu_y < 0$ as a reflection of Sigmund's instability, the last term on the right hand side has been introduced *ad-hoc* [8] in order to stabilize the system so that disturbances do not increase exponentially without bound for arbitrarily small length-scales. As shown by

Mullins [9], this fourth order derivative term describes isotropic surface diffusion, and here it leads to a ripple wavelength that is tens and up to hundred times a [8], as experimentally seen. Other predictions of BH's equation (like ripple orientation as a function of θ and various other dependences with experimental parameters) coincide to a large extent with experimental observations, as has been reviewed recently [2,3].

Working still within a linear approximation to the surface height in a similar spirit to the introduction of surface diffusion above, some alternative physical mechanisms have been proposed, specially in order to account for the lack of pattern (ripple) formation at either low temperatures T or small θ [10]. Thus, a term of the form $-F|k|h(k, t)$ added to the (Fourier transformed) right hand side of Eq. (1) can describe the effect of bulk viscous flow onto the surface dynamics, with F depending on the surface free energy and bulk viscosity [9]. For low enough T at which thermal surface diffusion is hampered, bulk viscous flow could dominate the surface dynamics even to the extent of preventing ripple formation for oblique incidence [10] or dot formation for rotating substrates [11,12]. Alternatively, the fact that a fraction of the sputtered atoms that move close to the surface are recaptured has led to arguing [13] for the inclusion of a term with the form $\nu_{recc}\partial_x^2 h$, where ν_{recc} would be a positive, angle dependent coefficient. We will see later a natural description of local redeposition effects.

Indeed, BH's linear theory already predicts many important features of IBS nanopatterning, but leaves out a number of additional properties. For instance, it cannot predict saturation of the ripple amplitude or their non-uniform lateral motion. In order to account for these, one needs to generalize the BH theory, the most natural procedure being the extension of their perturbative expansion in surface derivatives up to higher order. Along the way, not only do non-linear contributions arise, but also corrections appear to previous linear terms. These thus provide contributions of erosive origin to linear relaxation mechanisms such as transverse pattern motion, and surface diffusion. This program has been carried out in [14-16] with the result

$$\begin{aligned}\partial_t h = &-v_0 + \gamma_x \partial_x h + \Omega_1 \partial_x^3 h + \Omega_2 \partial_x \partial_y^2 h + \xi_x \partial_x h \partial_x^2 h + \xi_y \partial_x h \partial_y^2 h \\ &+ \nu_x \partial_x^2 h + \nu_y \partial_y^2 h + \lambda_x (\partial_x h)^2 + \lambda_y (\partial_y h)^2 - D_{xx} \partial_x^4 h - D_{yy} \partial_y^4 h - D_{xy} \partial_x^2 \partial_y^2 h,\end{aligned} \tag{2}$$

where all coefficients depend on the experimental parameters from Sigmund's theory [16], like in BH's equation (1), which now becomes a linear, low order approximation of (2). In the first line of the latter, and except for the constant average velocity $-v_0$, all terms contribute to the transverse ripple motion. The second line reflects the dependence of the sputtering yield with local curvatures and slopes, and contains surface diffusion terms that include thermal (as in BH) and erosive contributions. In (2) there is no inversion symmetry in x due to the ion beam, dependence of all parameters on θ being such that, for normal incidence $\theta = 0$, $D_{xx} = D_{yy} = D_{xy}/2$, $\nu_x = \nu_y \equiv \nu < 0$, $\lambda_x = \lambda_y \equiv \lambda_0$, $\gamma_x = \xi_x = \xi_y = \Omega_1 = \Omega_2 = 0$ [16], rotational symmetry is restored, and (2) becomes the celebrated Kuramoto-Sivashinsky (KS) equation

$$\partial_t h = -v_0 + \nu \nabla^2 h - D \nabla^4 h + \lambda_0 (\nabla h)^2. \tag{3}$$

The main morphological implications of (2), (3) have been discussed elsewhere [16]. Briefly, the BH behavior appears as a short-time transient, and all predictions —the dependence of e.g. the ripple structure with θ— still carry over here. Moreover, for temperatures at which surface

diffusion is activated, the dependences of the ripple wavelength *l* with energy, temperature and flux are as in BH, at least for short to intermediate times. If *T* is low enough that the only contribution to surface diffusion is from erosive origin, these dependences are modified and compare better with experiments [16]. For intermediate to long times, the nonlinear terms in Eqs. (2), (3) are such that the exponential growth of the ripple amplitude is stabilized, yielding to a much slower power-law increase of e.g. the surface roughness with time. At normal incidence, the surface displays kinetic roughening for long time and length scales, and this is also the case at oblique incidence, as long as coefficients λ_x, λ_y have the same signs. Otherwise, Eq. (2) features *cancellation modes* as first identified in the anisotropic KS equation, that is the particular case of (2) in which the propagative terms with coefficients ξ_i, Ω_i (being irrelevant to saturation of the ripple amplitude) are simply dropped out [14,17]:

$$\partial_t h = -\nu_0 + \gamma_x \partial_x h + \nu_x \partial_x^2 h + \nu_y \partial_y^2 h - D_{xx} \partial_x^4 h - D_{yy} \partial_y^4 h - D_{xy} \partial_x^2 \partial_y^2 h + \lambda_x (\partial_x h)^2 + \lambda_y (\partial_y h)^2. \qquad (4)$$

Cancellation modes are height Fourier modes with wave vector in the unstable band, for which the non-linear terms cancel each other, leaving the system non-linearly unstable, and inducing ripples which are oriented in an oblique direction that is parallel neither to the *x* nor to the *y* axis [17]. Eq. (3) has, on the other hand, the capability [beyond linear equations such as (1)] of predicting both "dot" and "hole" production, depending on the sign of the λ_0, which in turn depends on the characteristics of Sigmund's distribution [18]. However, conspicuous nonlinear features still remain beyond description by the KS equation (3) and its generalizations (2), (4). First, the predicted "dot" or ripple structures are characterized by a wavelength that remains fixed in time for any parameter values, so that experiments in which coarsening occurs cannot be accounted for. A stronger limitation is that the patterns described by (2)-(4) disorder in heights to the extent that there is no proper lateral ordering. Actually, the KS equation is known as a paradigm of spatio-temporal chaos in the field of Non-Linear Science. Following the program sketched at the beginning of this paragraph, a natural step is to carry on further the perturbative study of Sigmund's local velocity of erosion. At the present stage, one could close Eq. (2) (we consider $\theta = 0$ for simplicity) by including non-linear terms that are quadratic in the height field and fourth order in space derivatives, reaching an equation like (in a suitable reference frame)

$$\partial_t h = \nu \nabla^2 h - D \nabla^4 h + \lambda_1 (\nabla h)^2 + \lambda_2 \nabla^2 (\nabla h)^2. \qquad (5)$$

Indeed, such a higher order generalization has been performed [19]. However, the expressions of λ_1 and λ_2 in terms of Sigmund's parameters are such that the coefficients of the two nonlinear terms in (5) have the same signs for all physical values. Unfortunately, as shown shortly after [20,21], this introduces cancellation modes that seriously question the mathematical validity of (5) for our physical system: working Fourier space, we have

$$\partial_t h(\vec{k}) = (-\nu k^2 - D k^4) h(\vec{k}) + (\lambda_1 - \lambda_2 k^2) FT(\nabla h)^2, \qquad (6)$$

where *FT* denotes Fourier Transform. For the unstable mode $\vec{k}_0$ (that indeed occurs physically, see the experiments of IBS of Pd(001) in [19,20]) such that $k_0^2 = \lambda_1 / \lambda_2$, the nonlinear terms

cancel each other, and the amplitude of this mode blows up exponentially. We are seemingly left with a matter-of-principle limitation, namely, the theoretical approach based on Sigmund's local velocity of erosion meets (at sufficiently high linear and non-linear orders) mathematical limitations before being able to cover for the various relevant experimental features. In the following paragraph we will take a wider viewpoint in which the dynamics is more complete, in the sense that the surface height will be coupled to an additional physical field describing the flux of adsorbed material that diffuses on the near-surface layer. This procedure will be seen to provide an improved description solving some of the above physical and mathematical shortcomings. Before doing so, we note that additional studies exist that focus on the evolution of the height field only. Thus, the well-known result in the field of Pattern Formation (see references in [22]) that a linear damping in the KS equation induces ordered patterns, has directly led to the proposition [23] of a (modified) damped KS equation, that actually becomes the standard damped KS equation after a non-local time transformation [24]. Although the natural anisotropic generalization has been duly proposed [25], these equations unfortunately do not improve much one-field continuum descriptions for several reasons: (i) there is no connection to phenomenological parameters (the equations are not *derived* from any model but are, rather, argued for on a phenomenological basis); (ii) damped generalizations of the KS equation are known (see [26] and references therein) *not* to allow for wavelength coarsening for any parameter values, which leaves out of these descriptions many of the experimentally observed patterns; (iii) similarly, at long times the fluctuations of the height Power Spectral Density (PSD) function predicted by any of the damped generalizations of the KS equation are cut-off and do not show the power-law behavior that is seen, even in experiments in which there is no coarsening [27]. In contrast, a more successful extension of the BH-type approach has been its generalization [6] to surfaces with steep slopes. Recall that, starting with BH's, all considered continuum approaches (in contrast e.g. with MC models) work within a small-slope approximation. Remarkably, a suitable generalization for arbitrary slope values has been seen [6] to lead to a non-linear equation whose travelling wave (shock) solutions compare well with the experimental motion of the walls of pits excavated by a FIB. These results possibly provide important clues for a more complete model of nanopatterning by IBS.

TWO FIELD MODELS

The previous section leaves us with the need to enlarge the continuum description of nanopatterning by IBS. The expectation is that, by incorporating the dynamics of additional physically relevant fields, the effective height equation to be eventually derived improves its formal properties and its predictive power. Perhaps we could compare the situation with related fields such as e.g. the growth of thin films by physical or chemical vapor deposition (CVD) techniques. In CVD, for instance (see references in [4]), the standard continuum description arises precisely from the coupling between the local growth velocity and the dynamics of the concentration field of the diffusing species that eventually will stick to the growing aggregate. There have been various attempts in the IBS context to combine the surface dynamics as predicted by a BH-type equation, with the evolution of relevant surface species, such as adatoms, addimers and surface traps (see [28] and references therein). However, in this approach no explicit feedback mechanism is provided from the dynamics of such species onto the local variation of the surface height so that the dynamics cannot be described by a closed system of equations. On the other extreme, there is a recent proposal in which a full Navier-Stokes (thus, highly coupled) formulation is proposed to describe ripple transverse motion onto a glass surface

[29]. Trying to reach a balance between complexity and completeness in the physical description, one can seek for a formulation that, while simpler than a full hydrodynamic model, still provides an explicit coupling between the surface topography and the evolution of the relevant diffusive fields. For the case of ripple dynamics in the different (macroscopic!) context of aeolian sand dunes [30], such is the spirit of the so-called "hydrodynamic" approach, in which one sets up a system of coupled equations that describe the height of the eroded substrate profile, h, and the thickness of a mobile surface layer, R. Although there are relevant differences between both physical systems —the size of the structures is seven orders of magnitude larger in aeolian ripple formation than in IBS—, the many qualitative similarities between them suggest that these processes could be modelled by similar formalisms. This program has been followed in Refs. [31-34], where the next system is proposed to describe the evolution of h and R

$$\begin{aligned} \partial_t h &= -\Gamma^{ex} + \Gamma^{ad}, \\ \partial_t R &= (1-\phi)\Gamma^{ex} - \Gamma^{ad} - \nabla \cdot \vec{J}. \end{aligned} \tag{7}$$

In (7), $\Gamma^{ex}(h,R)$ and $\Gamma^{ad}(h,R)$ are, respectively, rates of atom excavation from and addition to the immobile bulk (h), $1-\phi$ measures the fraction of eroded atoms that become mobile but not sputtered, and the flux $\vec{J} = -D\nabla R$ describes diffusive mass transport onto the surface, where D is a thermally activated constant. In this way, local redeposition [35] is allowed if $\phi \neq 1$, while the viscous near-surface [36] layer R is provided with a dynamics of its own. In [31,32], a linear dependence of Γ^{ex} and Γ^{ad} with the local surface geometry is considered to study the linear stability of the system. These studies reveal that depending on parameter values, the ripple orientation could be aligned in any target direction, one of the limitations of these models being their ill-defined zero-redeposition $\phi = 1$ limit. More detailed mechanisms of erosion and addition are provided in [33,34], that are seen below to induce richer pattern dynamics than previous one-field models. Unlike Aste-Valbusa's and aeolian sand ripples models, in [33,34] direct knock-on of superficial atoms is neglected. Another feature of [33,34] is the presence of a non-zero amount of mobile material, R_{eq}, even in the absence of excavation ($\Gamma^{ex} = 0$) o redeposition ($\phi = 1$), which can be thermally induced. This term allows us to write Γ^{ad} in a form similar to the Gibbs-Thompson formula for surface relaxation by evaporation-condensation [37], namely,

$$\Gamma^{ad} = \gamma_0[R - R_{eq}(1 - \gamma_{2x}\partial_x^2 h - \gamma_{2y}\partial_y^2 h)], \tag{8}$$

where γ_0 is the mean nucleation rate for a flat surface and γ_{2x}, γ_{2y} describe variations of the nucleation rate with surface curvatures (being positive if nucleation events are more likely in surface valleys than in protrusions). In [34,37], a similar expression to the non-linear generalization (2) of BH's local erosion velocity is considered for Γ^{ex}:

$$\Gamma^{ex} = \alpha_0 \left\{ 1 + \alpha_{1x}\partial_x h + \sum_{j=x,y} \left[\left(\alpha_{2j} + \alpha_{3j}\partial_x + \alpha_{5j}(\partial_x h) + \sum_{i=x,y} \alpha_{4ij}\partial_i^2 \right)(\partial_j^2 h) + \alpha_{6j}(\partial_j h)^2 \right] \right\}, \tag{9}$$

where parameters reflect the dependence of the excavation rate on the *local* shape of the surface and are functions of experimental parameters, just as the coefficients of Eq. (2).

Oblique incidence

The time scale separation we have mentioned is seen to play a crucial role in (7). Thus, the diffusive field *R* relaxes much faster than the target height *h*, making it possible within a multiple-scale formulation to solve perturbatively for the dynamics of the former and derive a closed effective equation for the evolution of the latter which, for $\theta \neq 0$, reads [34,37]

$$\partial_t h = -v_0 + \gamma_x \partial_x h + \sum_{i=x,y} [\nu_i \partial_i^2 h + \lambda_i^{(1)} (\partial_i h)^2 + \Omega_i \partial_x \partial_i^2 h + \xi_i \partial_x h \partial_i^2 h] - \sum_{i=x,y} [D_{ij} \partial_i^2 \partial_j^2 h - \lambda_{ij}^{(2)} \partial_i^2 (\partial_j h)^2], \tag{10}$$

where these new coefficients depend on those in (7)-(9). As in the nonlinear continuous theories shown above, reflection symmetry is broken in *x*, being preserved in the *y* axis. Eq. (10) generalizes the height equations in [8,16], the main difference with (2) being the terms $\lambda_{ij}^{(2)}$, that turn out to be crucial to improve the description of the pattern, as seen below. To the best of our knowledge, Eq. (10) is new, and indeed has a rich parameter space. Numerical integration within linear regime retrieves all BH features of the ripple structure, such as dependence of l with linear terms, and ripple orientation as a function of θ. Top views of the morphologies described by Eq. (10) at different times are shown in panels (b1) and (b2) of Fig. 1.

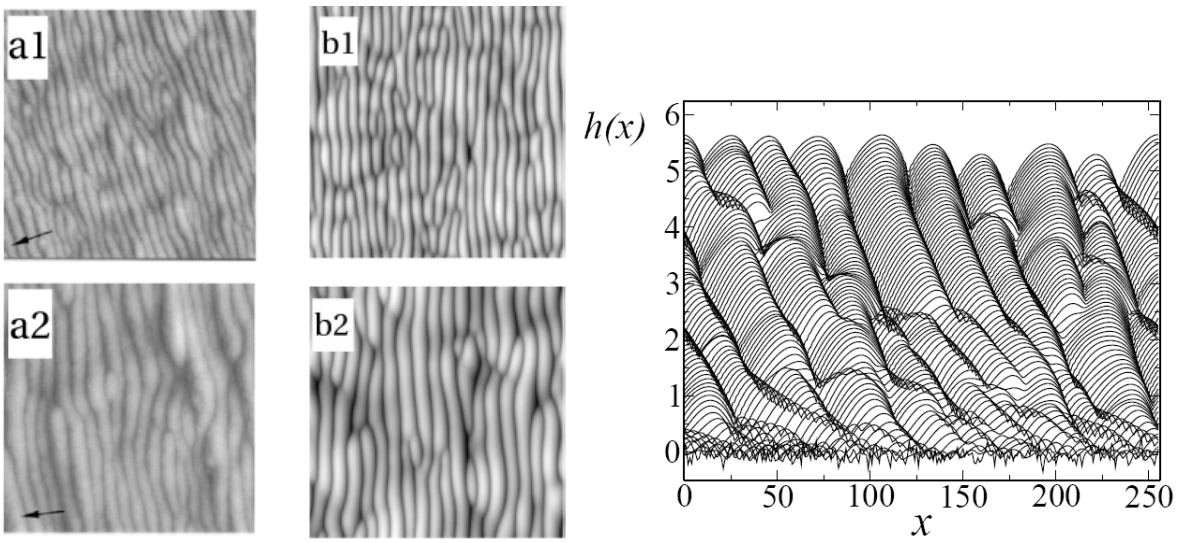

Figure 1. (a1-2): 1x1 μm^2 AFM top views of fused silica targets after 10 and 60 min. sputtering [38]. (b1-2) Numerical morphologies from (10) at times t_1 and $6t_1$. (c) Lateral cuts at equally spaced times for a numerical simulation of Eq. (10). Non uniform lateral translation can be seen.

The ripples increase in wavelength with time while disordering in heights for long distances, whereas the form of the ripples can vary appreciably depending on parameter values. The ripple coarsening seen in Fig. 1 requires the presence of $\lambda_{ij}^{(2)}$, whose magnitude and mathematically correct sign are due to having described redeposition through the additional field *R*. When the

values of these coefficients increase relative to $\lambda_i^{(1)}$, coarsening stops later, and the amplitude and wavelength of the pattern also increase, analogous to the result for one-dimensional interfaces studied in [39]. The coarsening exponent *n* in $l = t^n$ will take an *effective* value that will be larger the later coarsening stops and depends on parameter values [39].

Ripple asymmetry and transverse motion depend on terms with an odd number of derivatives in (10). Whereas the linear term γ_x tends to make the ripples move with a constant velocity, Ω_i and ξ_i induce non-uniform movement as experimentally observed [29,40]. In Fig. 1 right we show the evolution of lateral cuts of the surface as described by Eq. (10), where both non-uniform motion and asymmetry can be seen. Comparison of (10) with experiments is provided by panels (a1) and (a2) in Fig. 1, in which ripple coarsening is again clear. As we see, Eq. (10) indeed captures essential properties of the evolution of experimental topographies.

Normal incidence and rotating targets

For $\theta = 0$, the in-plane asymmetry due to the oblique beam disappears and, for materials that do not show privileged directions, the effective interface equation [33,34,37] coincides with Eq. (5) where, again, the coefficients are related to the Sigmund's parameters (a stochastic generalization of this equation has been also proposed in the context of amorphous thin film growth [41]). *However*, for generic redeposition conditions ($0 < \phi < 1$), $\lambda^{(1)}$ and $\lambda^{(2)}$ have *different signs*, so that the model is now free of cancellation modes. In the absence of redeposition ($\phi = 1$), cancellation modes do reappear, as expected from the purely erosive approach [19] discussed above. Hence, the description with a single height field seems to feature an intrinsic problem which is solved, for large enough redeposition, through the two-field approach.

In order to simplify the analysis of (5) within our present model, as in the one-dimensional counterpart of (5) studied in [39], we rescale (*x,y*), *t*, and *h* by $\left(D/\nu\right)^{1/2}$, D/ν^2, and $\nu/\lambda^{(1)}$, respectively, resulting into the single-parameter equation

$$\partial_t h = -\nabla^2 h - \nabla^4 h + (\nabla h)^2 - r\nabla^2 (\nabla h)^2, \qquad (11)$$

where $r = -(\nu\lambda^{(2)} / D\lambda^{(1)})$ is a *positive* parameter which allows us to perform a numerical analysis of the complete parameter space of Eq. (5). In general, starting from an initial random profile, a periodic surface structure with a wavelength of about the maximum of the linear dispersion relation arises and the amplitude of *h* increases. Then, coarsening occurs and dots grow in width and height, the total number of them decreasing. The shape of *l(t)* is shown in Fig. 2 (left) where saturation of ripple wavelength can be observed at long times. Simultaneously with dot coarsening, in-plane order eventually increases leading to an hexagonal dot array like those marked (b1) and (b2) in the same figure. As an example of comparison of Eq. (5) with specific experiments, we now consider recent results [42] where nanodots arrays are obtained over Si(001) and Si(111) targets irradiated at $\theta = 0$ with 1.2 keV Ar^+ ions.

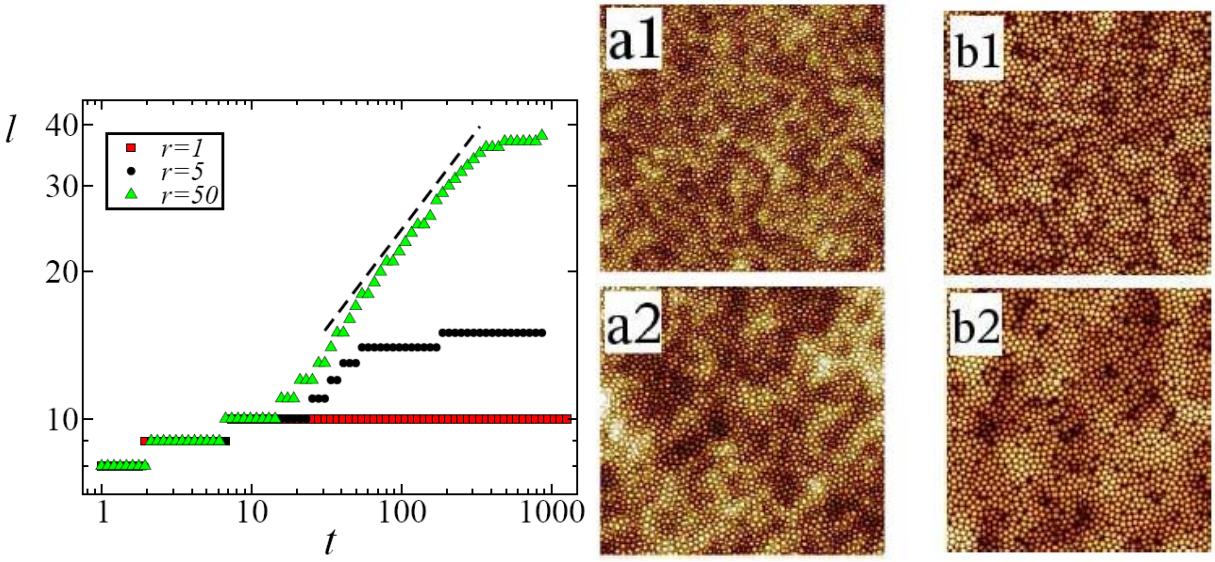

Figure 2. (Left) Ripple wavelength vs time for Eq. (11) and several r values. The dashed line corresponds to $l = t^{0.4}$. (Right) 3x3 μm^2 AFM images of Si(100) sputtered as in [41] after 60 min. (a1) and 960 min. (a2). Results of numerical integration of (5) for t_2 (b1) and $16t_2$ (b2).

For illustration we show in Fig. 2(a1-2) characteristic AFM images for the Si(001) case at two different times. The pattern is similar in both experiments: dots of 5-7 nm high and 40-60 nm wide are formed and group into short-range hexagonal order. For $t > 20$ min, height disorder occurs for large distances (roughly 6 nm in height and 500 nm across). This long-range disorder (kinetic roughening) increases with time. The rate of erosion was determined experimentally by partially masking samples during sputtering and measuring the resulting step edge height with a profilometer. The sputtering rate (SR) was 10% higher for Si(111) than for Si(001). In order to understand these differences between the two surface orientations, we have integrated Eq. (5) numerically. As the model neglects target crystallinity, we have used the relative difference in SR to simulate pattern evolution in two model systems. We provide in Fig. 2(b1-2) results of simulations for a surface with a 10% lower SR, thus representing the Si(100) orientation. The simulations reproduce in both cases the experimental coarsening and occurrence of a long wavelength corrugation. The wavelength l is seen to saturate earlier for the surface with higher SR, but the lower SR case attains a larger final dot size. In addition, the correlation length also saturates earlier for a higher SR. Remarkably, both AFM and simulation results agree in estimating ordered domains to reach roughly three nanodots across. This agreement between simulations and experiments allows us to conclude that the differences observed between the pattern evolution on Si(111) and Si(001) surfaces are due to their different SRs.

Finally, following Ref. [12], in Ref. [34,37] we have obtained the evolution equation for the surface in case the substrate is rotated simultaneously with irradiation, that reads

$$\partial_t h = \nu_r \nabla^2 h - D_r \nabla^4 h + \lambda_r^{(1)} (\nabla h)^2 + \lambda_r^{(2)} \nabla^2 (\nabla h)^2 + \lambda_r^{(3)} \nabla \cdot \left[\left(\nabla^2 h \right) \nabla h \right], \qquad (12)$$

where parameters are functions of those in (10). Simulations of (12) [37] show that this equation also presents interrupted coarsening and an ordered dot array, in which the morphological effect of the new term with coefficient $\lambda_r^{(3)}$ is similar to that of $\lambda_r^{(2)}$.

CONCLUSIONS

The continuum description of nanopattern formation by IBS is currently still open and making progress. As seen above, to date there are several alternative descriptions available that share some of their predictions, while differing in several other aspects. Theoretical work is not even complete yet —in terms of analyzing systematically the dependences of morphological properties with physical parameters— due to two main reasons: (i) the main interfacial equations are nonlinear, thus not easily amenable to analytical solutions, while some of the physically interesting features such as the stationary pattern wavelength or the direction of transverse ripple motion depend crucially on non-linear effects; (ii) the parameter spaces of these models are large, particularly in the oblique-incidence case. Actually, some of the interface equations that we have been considering seem to be new in the wider contexts of Non-equilibrium Systems and Non-linear Dynamics [4,26,39] even to the extent of providing examples of thus far unknown behaviors for problems of high current interest, like coarsening. While the two-field model leading to Eqs. (10)-(12) seems to date the theoretical description that can account for a larger range of experimental behaviors from within a single framework, much more work is still needed in order to reach a description of these physical systems with yet increased predictive power.

ACKNOWLEDGMENTS

Our work has been partially supported by Spanish grants Nos. FIS2006-12253-C06 (-01, -02, -03, -06) from Ministerio de Educación y Ciencia (MEC), CCG06-UAM/MAT-0040 from Comunidad Autónoma de Madrid (CAM) and Universidad Autónoma de Madrid, UC3M-FI-05-007 and CCG06-UC3M/ESP-0668 from CAM and Universidad Carlos III de Madrid, and S-0505/ESP-0158 from CAM, and by the Ramón y Cajal programme of MEC (R. G.).

REFERENCES

1. U. Valbusa, C. Boragno and F. Buatier de Mongeot, *J. Phys: Condensed Matter* **14**, 8153 (2002).
2. W. L. Chan and E. Chason, *J. Appl. Phys.* **101**, 121301 (2007).
3. J. Muñoz-García, L. Vázquez, R. Cuerno, J. A. Sánchez-García, M. Castro and R. Gago, "Self-organized surface nanopatterning by ion beam sputtering," *Lecture Notes on Nanoscale Science and Technology* (Springer, in press. arXiv:0706.2625v1).
4. R. Cuerno, M. Castro, J. Muñoz-García, R. Gago and L. Vázquez, *Eur. Phys. J. Special Topics* **146**, 427 (2007).
5. P. Sigmund, *J. Mat. Sci.* **8**, 1545 (1973).
6. H. H. Chen, O. A. Urquidez, S. Ichim, L. H. Rodriguez, M. P. Brenner and M. J. Aziz, *Science* **310,** 294 (2005).
7. M. Feix, A. K. Hartmann, R. Kree, J. Muñoz-García and R. Cuerno, *Phys. Rev.* **B71**, 125407 (2005).
8. R. M. Bradley and J. M. E. Harper, *J. Vac. Sci. Technol.* **A6,** 2390 (1988).

9. W. W. Mullins, *J. Appl. Phys.* **28**, 333 (1957).
10. E. Chason, T. M. Mayer, B. K. Kellerman, D. T. McIlroy and A. J. Howard, *Phys. Rev. Lett.* **72**, 3040 (1994).
11. E.-H. Cirlin, J. J. Vajo, R. E. Doty and T. C. Hasenberg, *J. Vac. Sci. Technol.* **A9** 1395 (1991).
12. R. M. Bradley, *Phys. Rev.* **E54**, 6149 (1996).
13. G. Carter and V. Vishnyakov, *Phys. Rev.* **B54**, 17647 (1996).
14. R. Cuerno and A.-L. Barabási, *Phys. Rev. Lett.* **74**, 4746 (1995).
15. M. A. Makeev and A.-L. Barabási, *Appl. Phys. Lett.* **71**, 2800 (1997).
16. M. A. Makeev, R. Cuerno and A.-L. Barabási, *Nucl. Instrum. Meth.* **B97**, 185 (2002).
17. M. Rost and J. Krug, *Phys. Rev. Lett.* **75,** 3894 (2005).
18. B. Kahng, H. Jeong and A.-L. Barabási, *Appl. Phys. Lett.* **78**, 805 (2001).
19. T. C. Kim, C.-M. Ghim, H. J. Kim, D. H. Kim, D. Y. Noh, N. D. Kim, J. W. Chung, J. S. Yang, Y. J. Chang, T. W. Noh, B. Kahng and J.-S. Kim, *Phys. Rev. Lett.* **92**, 246104 (2004).
20. M. Castro and R. Cuerno, *Phys. Rev. Lett.* **94**, 139601 (2005).
21. T. C. Kim, C.-M. Ghim, H. J. Kim, D. H. Kim, D. Y. Noh, N. D. Kim, J. W. Chung, J. S. Yang, Y. J. Chang, T. W. Noh, B. Kahng and J.-S. Kim, *Phys. Rev. Lett.* **94**, 139602 (2005).
22. M. Paniconi and K. R. Elder, *Phys. Rev.* **E56**, 2713 (1997).
23. S. Facsko, T. Bobek, A. Stahl, H. Kurz and T. Dekorsy, *Phys. Rev.* **B69**, 153412 (2004).
24. S. Vogel and S. J. Linz, *Phys. Rev.* **B72**, 035416 (2005).
25. S. Vogel S and S. J. Linz, *Europhys. Lett.* **76**, 884 (2006).
26. M. Castro, J. Muñoz-García, R. Cuerno, M. García-Hernández and L. Vázquez , *New J. Phys.* **9**, 102 (2007).
27. B. Ziberi, F. Frost and B. Rauschenbach, *Surf. Sci.* **600,** 3757 (2006).
28. E. Chason, J. Erlebacher, M. J. Aziz, J. A. Floro and M. B. Sinclair, *Nucl. Instrum. Meth.* **B178**, 55 (2001).
29. P. F. A. Alkemade, *Phys. Rev. Lett.* **96**, 107602 (2006).
30. Z. Csahók, C. Misbah, F. Rioual and A. Valance, *Eur. Phys. J.* **E3**, 71 (2000).
31. T. Aste and U. Valbusa, *Physica* **A332**, 548 (2004).
32. T. Aste and U. Valbusa, *New. J. Phys.* **7** 122 (2005).
33. M. Castro, R. Cuerno, L. Vázquez and R. Gago, *Phys. Rev. Lett.* **94**, 016102 (2005).
34. J. Muñoz-García, M. Castro and R. Cuerno, *Phys. Rev. Lett.* **96**, 086101 (2006).
35 M. C. Moore, N. Kalyanasundaram, J. B. Freund and H. T. Johnson, *Nucl. Instrum. Meth.* **B225**, 241 (2004).
36 C. C. Umbach, R. L. Headrick and K. Chang, *Phys Rev Lett* **87**, 246104 (2001).
37. J. Muñoz-García, R. Cuerno and M. Castro, preprint (2007).
38. D. Flamm, F. Frost and D. Hirsch, *Appl. Surf. Sci.* **179**, 95 (2001).
39. J. Muñoz-García, R. Cuerno and M. Castro, *Phys. Rev.* **E74**, 050103(R) (2006).
40. S. Habenicht, K. P. Lieb, J. Koch and A. D. Wieck, *Phys. Rev.* **B65**, 115327 (2002).
41. M. Raible, S. G. Mayr, S. J. Linz, M. Moske, P. Hänggi and K. Samwer, *Europhys. Lett*. **50**, 61 (2000).
42. R. Gago, L. Vázquez, O. Plantevin, T. H. Metzger, J. Muñoz-García, R. Cuerno and M. Castro, *Appl. Phys. Lett*. **89,** 233101 (2006).